Radiographic imaging with cosmic-ray muons

Natural background particles could be exploited to detect concealed nuclear materials.

Despite its enormous success, X-ray radiography[1] has its limitations: an inability to penetrate dense objects, the need for multiple projections to resolve three-dimensional structure, and health risks from radiation. Here we show that natural background muons, which are generated by cosmic rays and are highly penetrating, can be used for radiographic imaging of medium-to-large, dense objects, without these limitations and with a reasonably short exposure time. This inexpensive and harmless technique may offer a useful alternative for detecting dense materials — for example, a block of uranium concealed inside a truck full of sheep.

In X-ray radiography, the intensity of an image pixel is determined by the attenuation of the incident beam caused by absorption and scattering — the maximum mean free path for photons is about 25 g cm^{-2} for all materials, corresponding to less than 2 cm of lead. For thicker objects, it is better to use a different type of radiography that is based on the interaction of charged particles with matter by multiple Coulomb scattering. The many small interactions add up to yield an angular deviation that roughly follows a gaussian distribution,

$$\frac{dN}{d\theta_x} = \frac{1}{\sqrt{2\pi}\theta_0} e^{-\frac{\theta_x^2}{2\theta_0^2}}$$

with the width, θ_0, related to the scattering material through its radiation length, L_0, as follows:

$$\theta_0 = \frac{13.6}{\beta cp}\sqrt{\frac{L}{L_0}}[1 + 0.038\ln(L/L_0)]$$

where p is the particle's momentum in MeV c^{-1} and βc is its velocity[2]. The radiation length decreases rapidly as the atomic number of a material increases, and θ_0 increases accordingly: in a layer 10 cm thick, a 3-GeV muon will scatter with an angle of 2.3 milliradians in water, 11 milliradians in iron and 20 milliradians in lead. By tracking the scattering angles of individual particles, the scattering material can be mapped.

Our new technique relies on the scattering of atmospheric muons produced by primary cosmic rays. Muons are the most numerous cosmic-ray particles at sea level, moving at a rate of about 10,000 m^{-2} min^{-1} in horizontal detectors[3]. These particles are highly penetrating: a typical cosmic-ray muon of energy 3 GeV will penetrate more than 1,000 g cm^{-2} (10 m of water, for example).

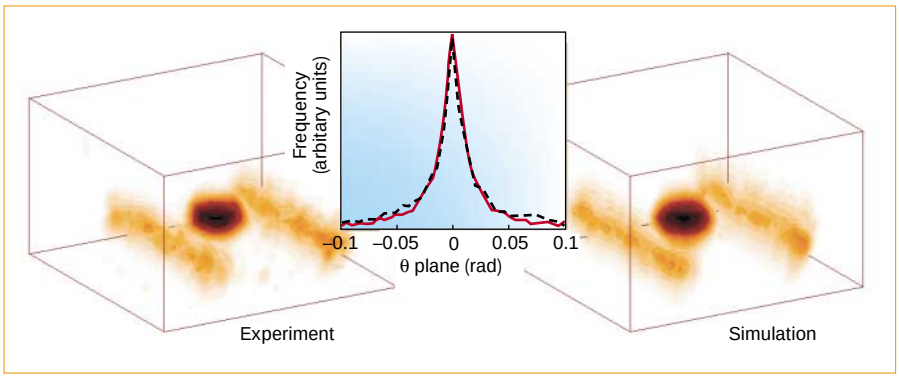

Figure 1 Radiographic imaging with muons of a test object (left) and the reconstructed image of its Monte Carlo simulation (right). The test object is a tungsten cylinder (radius, 5.5 cm; height, 5.7 cm) on a plastic ($35 \times 60 \times 1$ cm^3) plate with two steel support rails. The tungsten cylinder and the iron in the rails are clearly visible in both the experiment and simulation reconstructions. Inset, the widths of the scattering distributions for tracks passing through the tungsten target are very similar for the experimental and simulated data.

To demonstrate the concept of muon radiography, we developed a small-scale experimental system with four drift chamber detectors[4] spaced 27 cm apart. Each detector has an active area of 60×60 cm^2 and records particle tracks at two positions in each of two orthogonal coordinates. The upper pair of detectors records the tracks of incident muons, and the lower pair records the scattered tracks. A tungsten cylinder was used as a test object, supported by a plastic plate and steel support beams. The tungsten is clearly visible in the reconstructed image, and the steel support beams are also evident (Fig. 1, left).

We also developed a Monte Carlo simulation code that generated cosmic-ray muons and propagated them through a test volume. The reconstructed images are indistinguishable from those obtained experimentally (Fig. 1), and the scatter angles of the simulated muons from the different materials (tungsten, lexan and steel) are consistent with the measured angles.

Simulation of larger, more complex objects demonstrates that we can reliably detect a $10 \times 10 \times 10$ cm^3 uranium object inside a large metal container full of sheep in 1 min of exposure. We conclude that cosmic-ray muons show promise as an inexpensive, harmless probe for radiography of medium-to-large objects, such as commercial trucks, passenger cars or sea containers. Our experimental results and simulations demonstrate the ability to reconstruct complex objects and to detect dense material of high atomic number hidden in a much larger volume of material of low atomic number, using only the natural flux of muons. This method is suitable for a range of practical applications in which radiography of dense objects with low radiation dose is required — for example, in surveillance for cross-border transport of nuclear materials.

Konstantin N. Borozdin, Gary E. Hogan, Christopher Morris, William C. Priedhorsky, Alexander Saunders, Larry J. Schultz, Margaret E. Teasdale

Los Alamos National Laboratory, Los Alamos, New Mexico 87545, USA

e-mail: kbor@lanl.gov

1. Roentgen, W. C. *Nature* **53,** 274 (1896).
2. Hagiwara, K. *et al. Phys. Rev. D* **66**, 01001 (2002).
3. Grieder, P.K.F. *Cosmic Rays at Earth* (Elsevier Science, Amsterdam, 2001).
4. Atencio, L. G., Amann, J. F., Boudrie, R. L. & Morris, C. L. *Nucl. Instr. Methods Phys. Res.* **187,** 381–386 (1981).

Competing financial interests: declared none.

Palaeo-oceanography

Deepwater variability in the Holocene epoch

The conversion of surface water to deep water in the North Atlantic results in the release of heat from the ocean to the atmosphere, which may have amplified millennial-scale climate variability during glacial times[1] and could even have contributed to the past 11,700 years of relatively mild climate (known as the Holocene epoch)[2–4]. Here we investigate changes in the carbon-isotope composition of benthic foraminifera throughout the Holocene and find that deep-water production varied on a centennial–millennial timescale. These variations may be linked to surface and atmospheric events that hint at a contribution to climate change over this period.

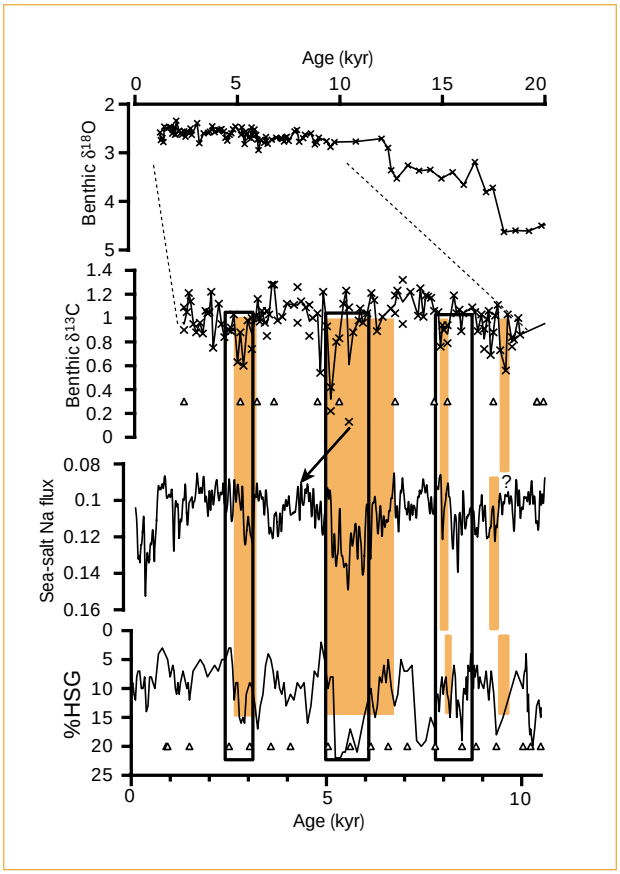

Figure 1 Holocene climate records, top to bottom: benthic $\delta^{18}O$ and $\delta^{13}C$ (North Atlantic deepwater contribution) records from site 980 (ref. 12, and see supplementary information); GISP2 sea-salt sodium flux[8] (increasing, calm to windier), and percentage of haematite-stained grains (%HSG) in core V29-191 (ref. 2). Triangles, dated levels in sediment cores; arrow marks the onset and intensificatoin of the 5-kyr event. Accelerator mass-spectrometer radiocarbon dates converted to calendar age[13] from site 980 provided the chronology for the Holocene (see supplementary information). Accumulation rates average about 25 cm kyr^{-1} in the Holocene, roughly double that in nearby core V29-191. The average interval between samples is about 100 yr from 9.7 to 1.2 kyr. Shading shows low-$\delta^{13}C$ events (see text) and possible correlative events in the other records; a more tenuous correlation is denoted by the question mark. Rectangles, extreme winter-like conditions deduced from statistical analysis of the full set of palaeochemical indicators from GISP2 (ref. 8).

We used an established deepwater proxy parameter — the carbon-isotope composition ($\delta^{13}C$) of the epifaunal benthic foraminifera *Cibicidoides wuellerstorfi*[5,6] — to evaluate Holocene deepwater variability. Variations in the $\delta^{13}C$ of the total amount of CO_2 in bottom waters, which is accurately recorded by *C. wuellerstorfi*, can be used to monitor variations in the contribution of high-$\delta^{13}C$ North Atlantic Deep Water (NADW) relative to low-$\delta^{13}C$ Southern Ocean Water (SOW) to a site. We worked on sediment from Ocean Drilling Project site 980 (55° N, 15° W; depth, 2,179 m), on the Feni Drift in the subpolar northeastern Atlantic.

Holocene $\delta^{13}C$ values (Fig. 1, and see supplementary information) show marked millennial oscillations around the modern value of about 1‰ (ref. 7). Values range from a high of 1.3‰ to values lower than 0.6‰, indicating times of enhanced and reduced NADW contribution, respectively. The largest reductions in the relative NADW contribution occurred around 9,300 years ago (9.3 kyr), and 8.0, 5.0 and 2.8 kyr ago. Smaller events occurred more frequently.

The most pronounced feature of the Holocene is a trend of decreasing relative NADW contribution that began at about 6.5 kyr and culminated with a minimum at around 5 kyr. Statistical analysis of the full set of chemical records from the Greenland Ice Sheet Project 2 (GISP2) ice core indicates that meteorological conditions from 6.1 to 5.0 kyr were especially winter-like (characterized by an expanded polar vortex) at high latitudes; this is consistent with high values of sea-salt sodium (Fig. 1) during this millennial-scale event[8].

A high relative abundance of haematite-stained grains in a nearby core indicates a large proportion of cold, fresh, ice-bearing surface water from north of Iceland[2]. All three records indicate that the 5-kyr event was the most severe climate event of our Holocene study interval. Apparently contemporary variations in benthic $\delta^{13}C$ and sea-salt sodium levels indicate that linked, century-scale variability may have occurred during this event.

The GISP2 palaeochemical records indicate enhanced winter-like conditions from 2.4 to 3.1 kyr, and from 8.8 to 7.8 kyr, although to a lesser extent than in the 5-kyr event[8]. The more recent of these cold intervals corresponds precisely to the reduced NADW contribution at around 2.8 kyr. The 8-kyr $\delta^{13}C$ minimum occurs late in the 8.8–7.8-kyr cold interval, but corresponds to a brief maximum in sea-salt sodium. The age of the 9.3-kyr event is poorly constrained, but it may correspond to one of several younger or older maxima in sea-salt sodium flux. Three of the four low-$\delta^{13}C$ events correspond to maxima in the percentage of haematite-stained grains (increased incursion of rock-bearing ice from north of Iceland), suggesting a possible surface–deepwater linkage.

Prior geochemical evidence for deepwater reduction in the Holocene was limited to events outside our study interval. Low $\delta^{13}C$ values during the Little Ice Age[4], the most recent of the Holocene millennial cold events[8], and during an early Holocene event at ~10.3 kyr (ref. 9) hint at a linkage between millennial climate and deep water. Downcore variations in sedimentological indices also indicate this possibility[10,11].

The new North Atlantic benthic $\delta^{13}C$ record unambiguously demonstrates that NADW varied on centennial–millennial time scales during the Holocene. The most significant Holocene event of reduced NADW contribution, which occurred at 5 kyr, was correlated to winter-like atmospheric conditions at high northern latitudes[8], and to incursion of sea ice from north of Iceland[2]. Similarly, a more recent cold event (at 3.1–2.4 kyr) was associated with a reduced NADW contribution.

Evidence for a climate–deepwater linkage during the earlier events is weaker, and may indicate an increasing sensitivity of deepwater to surface forcing from the Early to the Late Holocene. Further well-dated deepwater proxy records are needed to test this possibility.

Our study raises other important issues that can be addressed through data collection and modelling. The amplitude of the largest Holocene $\delta^{13}C$ fluctuation near 5 kyr, for example, is similar to those of $\delta^{13}C$ oscillations during earlier glacial and deglacial events[12]. This suggests that significant variations in the relative NADW contribution can occur in the absence of forcing by large ice sheets, and that NADW may be more sensitive to surface forcing than was previously imagined.

Delia W. Oppo*, Jerry F. McManus*, James L. Cullen†

**Department of Geology and Geophysics, Woods Hole Oceanographic Institution, Woods Hole, Massachusetts 02540, USA*
e-mail: doppo@whoi.edu
†*Department of Geological Sciences, Salem State College, Salem, Massachusetts 01970, USA*

1. Broecker, W. S., Bond, G. & Klas, M. *Paleoceanography* **5,** 469–477 (1990).
2. Bond, G. C. *et al. Science* **294,** 2130–2136 (2001).
3. Alley, R. B. *et al. Geology* **25,** 483–486 (1997).
4. Keigwin, L. D. & Boyle, E. A. *Proc. Natl Acad. Sci. USA* **97,** 1343–1346 (2000).
5. Curry, W. B., Duplessy, J. C., Labeyrie, L. D. & Shackleton, N. J. *Paleoceanography* **3,** 317–341 (1988).
6. Duplessy, J. C. *et al. Paleoceanography* **3,** 343–360 (1988).
7. Kroopnick, P. M. *Deep-Sea Res.* **32,** 57–84 (1985).
8. O'Brien, S. R. *et al. Science* **270,** 1962–1964 (1995).
9. Bond, G. C. *et al. Science* **278,** 1257–1266 (1997).
10. Bianchi, G. G. & McCave, I. N. *Nature* **397,** 515–517 (1999).
11. Chapman, M. R. & Shackleton, N. J. *Holocene* **10,** 287–291 (2000).
12. McManus, J. F., Oppo, D. W. & Cullen, J. L. *Science* **283,** 971–975 (1999).
13. Stuiver, M. & Braziunas, T. F. *Radiocarbon* **35,** 137–189 (1993).

Supplementary information accompanies this communication on *Nature*'s website.
Competing financial interests: declared none.